Performance comparison of dynamical decoupling sequences for a qubit in a rapidly fluctuating spin bath

Gonzalo A. Álvarez,[1,*] Ashok Ajoy,[1,2,3] Xinhua Peng,[1,4] and Dieter Suter[1,†]

[1]*Fakultät Physik, Technische Universität Dortmund, D-44221 Dortmund, Germany*
[2]*Birla Institute of Technology and Science, Pilani, Zuarinagar, Goa 403726, India*
[3]*NMR Research Centre, Indian Institute of Science, Bangalore 560012, India*
[4]*Hefei National Laboratory for Physical Sciences at Microscale and Department of Modern Physics,*
University of Science and Technology of China, Hefei, Anhui 230026, People's Republic of China

Avoiding the loss of coherence of quantum mechanical states is an important prerequisite for quantum information processing. Dynamical decoupling (DD) is one of the most effective experimental methods for maintaining coherence, especially when one can access only the qubit system and not its environment (bath). It involves the application of pulses to the system whose net effect is a reversal of the system-environment interaction. In any real system, however, the environment is not static, and therefore the reversal of the system-environment interaction becomes imperfect if the spacing between refocusing pulses becomes comparable to or longer than the correlation time of the environment. The efficiency of the refocusing improves therefore if the spacing between the pulses is reduced. Here, we quantify the efficiency of different DD sequences in preserving different quantum states. We use ^{13}C nuclear spins as qubits and an environment of ^{1}H nuclear spins as the environment, which couples to the qubit via magnetic dipole-dipole couplings. Strong dipole-dipole couplings between the proton spins result in a rapidly fluctuating environment with a correlation time of the order of 100 μs. Our experimental results show that short delays between the pulses yield better performance if they are compared with the bath correlation time. However, as the pulse spacing becomes shorter than the bath correlation time, an optimum is reached. For even shorter delays, the pulse imperfections dominate over the decoherence losses and cause the quantum state to decay.

I. INTRODUCTION

Quantum mechanical systems have an enormous potential for realizing information processing devices that are qualitatively more powerful than systems based on classical physics [1]. The main requirement for quantum information processing (QIP) is that the system evolves according to the Schrödinger equation, under the influence of a Hamiltonian that is under precise experimental control. However, no system is completely isolated, and disturbances from its surrounding environment (bath) spoil the quantum identity of the system. This process is often called decoherence [2] and limits the time scale over which quantum information can be retained and the distance over which it can be transmitted [3–5]. Reducing the effects of decoherence is therefore one of the main requirements for reliable quantum information processing. Several protocols have been developed for quantum error correction [6,7]; however, they prove advantageous only for low levels of environmental noise.

In all existing experimental architectures for QIP the noise background is too large, and this limits the applicability of these protocols. A promising technique for reducing the noise to a level where error-correcting codes can take over is called dynamical decoupling (DD) [8,9]. It aims to reduce the interaction of the system with the environment through control operations acting only on the system. It requires relatively modest resources, since it requires

no overhead of information encoding, measurements, or feedback.

Although the mathematical framework of dynamical decoupling was introduced fairly recently [8], the 6-decade-old Hahn NMR spin-echo experiment [10] can be considered the earliest and simplest implementation of this method. It consists of the application of a π pulse to a spin qubit ensemble at time τ after the spins were left to undergo Larmor precession in a magnetic field. This effectively reverses a pure dephasing system-environment (SE) interaction, i.e., one that does not cause a net exchange of energy between the system and the bath. The combined effect of the evolution before the refocusing pulse and a second period of the same duration after the pulse vanishes. Physically, the dephasing and rephasing of the spins can be observed as an apparent decay of the average magnetization in the system and a subsequent increase after the refocusing pulse (a spin echo).

The Hahn echo can (for an ideal pulse) completely eliminate the interaction with the environment, provided it is time invariant. In practice, this is often not the case, and a change in the environment reduces the refocusing efficiency [10,11]. To reduce the problems due to a time-dependent environment, Carr and Purcell suggested replacing the single pulse of the Hahn echo by a sequence of pulses at shorter intervals (the CP sequence) [11], thus reducing the changes in the environment between successive pulses. For sufficiently short pulse intervals, elimination of system-environment interactions became possible even in a time-dependent environment. However, the increased number of pulses led to another problem: If the refocusing pulses are not perfect, they actually become a source of decoherence (and thus signal loss) instead of

*galvarez@e3.physik.uni-dortmund.de
†Dieter.Suter@tu-dortmund.de

eliminating it. This problem was significantly reduced by a simple modification of the CP sequence: if the rotation axis of the refocusing pulses is parallel to the initial spin orientation, the effect of pulse errors is significantly reduced over a cycle [12]. This is known in literature as the Carr-Purcell-Meiboom-Gill (CPMG) sequence.

In the context of QIP, there has been renewed effort in eliminating the effects of the system-environment interaction that lead to the loss of quantum information. For this, it is often important that the refocusing reduces the effect of the system-environment interactions by several orders of magnitude. In addition, the effect of pulse errors must be minimized, and the sequence has to work for all possible initial states of the system. Several pulse sequences that achieve this were introduced [8,13–15], which consist of periodic sequences of pulses; they were thus called periodic DD (PDD). By design, they allow one to decouple the system from the environment for a general SE interaction, i.e., one that causes dephasing as well as dissipation.

Experimentally, DD is achieved by iteratively applying to the system a series of stroboscopic control pulses in cycles of period τ_c. Over that period, the time-averaged SE interaction Hamiltonian vanishes. The time average over τ_c can be calculated using average Hamiltonian theory [16]. If the average Hamiltonians are calculated by a series expansion, such as the Magnus expansion, improving the pulse sequence usually corresponds to progressively eliminating higher-order terms in the expansion. Khodjasteh and Lidar [17] introduced concatenated DD (CDD) as a scheme that recursively generates higher-order DD sequences for this purpose. Here, the lowest level of concatenation is a PDD sequence. The improvement achieved by concatenation comes at the expense of an exponential growth [17] in the number of applied control pulses. In contrast, for the case of a pure dephasing or pure dissipative interaction Hamiltonian [18,19], Uhrig developed a sequence (UDD) [20] that reduces higher orders in the Magnus expansion with only a linear overhead in the number of pulses. Unlike other DD sequences, in the UDD sequence the delay between successive pulses is not equal, i.e., the pulses are not equidistant. In the limit of a two-pulse cycle, UDD reduces to the CPMG sequence. Recent proposals of DD sequences that are a hybrid between UDD and CDD are predicted to improve DD performance of previous methods [21,22].

The UDD sequence was tested on ion traps [23,24], electron paramagnetic resonance [25], and liquid-state NMR [26] and found to outperform equidistant pulse sequences, in particular CPMG, for environments with a high-frequency or strong cutoff. CDD sequences were recently tested in solid-state NMR [27]. However, while some sequences for particular environmental noises were tested, a comparison between sequences for different kinds of environments is still missing. Most of the sequences were designed assuming ideal pulses and some of them predict to compensate pulse imperfection. However, an experimental test of this aspect is still needed. In parallel to this work recent DD implementations on a qubit interacting with a slowly fluctuating spin-bath were tested [28–32].

Other questions relate to the optimal cycle time: It is theoretically predicted and experimentally demonstrated that sequences that reduce higher-order terms of the Magnus expansion perform better than low-order sequences for slow motion environments with high-frequency or strong cutoff, when the bath correlation time τ_B is longer than the sequence time τ_c (cycle time). However, the strength and duration of control pulses are limited by hardware, yielding a minimum for the achievable DD cycle time. As some examples on this direction, Viola and Knill [15] and Gordon *et al.* [33] proposed a general method for DD with bounded controls. Khodjasteh and Lidar, keeping the delay between pulses constant, predicted an optimal CDD order for reducing decoherence [34,35]. Biercuk *et al.* [23,24] needed to consider the finite length of pulses in their simulations, assuming them perfect but producing a spin-lock during their application times, in order to fit them to the experiments. Additionally Hodgson *et al.* [36], while assuming instantaneous perfect pulses, theoretically analyzed DD performance constraining also the delay between pulses. They set a lower limit to the delays, making them larger than the pulse duration to satisfy the instantaneous pulse approximation in their theoretical model for experimental conditions. When the delays are strongly constrained, they predict that DD protocols like CDD or UDD, which are designed to improve the performance of lower DD orders if the regime of arbitrarily small pulse separations is achievable, in general lose their advantages. However, experiments are missing in order to demonstrate these predictions and very little is known about the performance of DD sequences under conditions where the cycle times are comparable to or longer than the bath correlation times. Recently Pryadko and Quiroz approached this regime but only for the extreme case of a Markovian environment [37].

While the finite length of pulses limits the minimum cycle time reducing the maximal achievable DD performance, their imperfections also contribute to reducing it. It is well know that CPMG-like sequences are too sensitive to the initial state when pulse errors are considered [13,14]. A comparisons between the CPMG and UDD sensitivity against pulse errors was performed in Ref. [24]. Overall UDD was shown to be more robust against flip angle errors and static offset errors, with the exception that CPMG is more robust for initial states longitudinal to the control pulses. But both of them are too asymmetric against initial state directions. In general, while some DD sequences were developed to compensate flip-angle errors and to have a performance more symmetric against initial conditions, an extensive study of their performance from a QIP perspective is still missing and additionally is not done for CDD sequences. For example, an optimal cycle time when considering imperfect finite pulses was predicted by Khodjasteh and Lidar [34].

In this article, we compare experimentally the performance of different DD sequences on a spin-based solid-state system where the cycle time τ_c is comparable to or longer than the correlation time τ_B of the environment. Here, the spin(qubit)-system interacts with a spin-bath where the spectral density of the bath is given by a normal (Gaussian) distribution. These kinds of systems, typical in NMR [38], are encountered in a wide range of solid-state systems, as, for example, electron spins in diamonds [30–32], electron spins in quantum dots [28,29,39], and donors in silicon [40,41], which appear to be promising candidates for future QIP implementations. In particular we consider the case where the interaction with the

bath is weak compared with the intrabath interaction. For one side the latter point complement and distinguish our work from the recent submitted articles [28–32]. For the other the aim of our work is a comprehensively and detailed comparison of the performance of different sequences considering different initial states. We find how the performance of the DD sequences depends on the initial state of the qubit ensemble with respect to the rotation axis of control pulses with finite precision. When they are in the same direction, the CPMG sequence is the best DD sequence for reducing decoherence, i.e., it maintains the state of the ensemble for the longest time. However, if the initial state of the ensemble is not known, we find that CDD provides the best overall performance. Stated equivalently, the CDD scheme provides the best overall minimization of the environmentally driven quantum mechanical evolution of the system. Additionally, we experimentally demonstrate and quantify the predicted optimal delay times for maximizing the performance of the respective DD sequences. This implies that pulse errors are a limiting factor that must be reduced to improve DD performances. In general our results complement some of the previous findings and predictions for some of the experimentally tested DD sequences and provide new results for untested ones. One of the main message is that a fair comparison of the performance of DD sequences should use a constant average number of pulses per unit time.

This article is organized as follows. Section II describes the qubit and bath system used in our experiment, and the mechanisms of coupling between them. In Sec. III we give a brief summary of dynamical decoupling and a description of the tested sequences: the Hahn echo, CPMG, PDD, CDD, and UDD. Our limited choice of sequences includes those most accepted by the QIP community and allows us to discuss the most important points. Section IV contains the experimental results and their analysis. In Sec. V we compare the various DD sequences under the same conditions. In the last section we draw some conclusions.

II. THE SYSTEM

Our system consists of a spin 1/2 (qubit) in a strong magnetic field oriented along the z axis, interacting with a bath consisting of a different type of spins 1/2. The total Hamiltonian in the laboratory frame is

$$\widehat{\mathcal{H}}^L = \widehat{\mathcal{H}}_S^L + \widehat{\mathcal{H}}_{SE}^L + \widehat{\mathcal{H}}_E^L, \tag{1}$$

where $\widehat{\mathcal{H}}_S^L$ is the system Hamiltonian, $\widehat{\mathcal{H}}_E^L$ is the environment Hamiltonian, and $\widehat{\mathcal{H}}_{SE}^L$ is the system-environment interaction Hamiltonian:

$$\widehat{\mathcal{H}}_S^L = \omega_S \hat{S}_z, \tag{2}$$

$$\widehat{\mathcal{H}}_{SE}^L = \hat{S}_z \sum_j b_{Sj} \hat{I}_z^j, \tag{3}$$

$$\widehat{\mathcal{H}}_E^L = \omega_I \sum_j \hat{I}_z^j + \sum_{i<j} d_{ij} \left[2\hat{I}_z^i \hat{I}_z^j - \left(\hat{I}_x^i \hat{I}_x^j + \hat{I}_y^i \hat{I}_y^j \right) \right], \tag{4}$$

where $\hat{S}$ is the spin operator of the system qubit, the spin operators $\hat{I}_x^j, \hat{I}_y^j$, and $\hat{I}_z^j$ act on the jth bath spin, ω_S and ω_I are the Zeeman frequencies of the system spin and the bath spins, respectively, and b_{Sj} and d_{ij} are the coupling

constants, and we use frequency units ($\hbar = 1$). In solids, the spin-spin interaction is dominated by the dipolar interaction [38]. Since S and I are different types of nuclei, it is possible to neglect the terms of the dipolar coupling Hamiltonian that do not commute with the strong Zeeman interaction because $|b_{Sj}|/|\omega_S - \omega_I| \ll 10^{-4}$ [38]. The remaining terms have the Ising form (3). Similarly, the homonuclear interaction between the bath spins is truncated to those terms that commute with the total Zeeman coupling, which we assume to be identical for all bath spins.

In the high-temperature thermal equilibrium [38], the density operator of the system spin is

$$\hat{\rho}_{S,\text{eq.}} \propto \hat{S}_z, \tag{5}$$

where we consider only the system (S spin) part of the total Hilbert space. We also neglect the part proportional to the unit operator, which does not evolve in time and does not contribute to the observable signal.

To generate the initial state for our DD measurements, we rotate the thermal state to the xy plane by applying a $\pi/2$ pulse. The resulting state is

$$\hat{\rho}_S(0) \propto \hat{S}_{\{ \begin{smallmatrix} x \\ y \end{smallmatrix} \}}. \tag{6}$$

For an isolated spin system this magnetization precesses indefinitely around the static magnetic field at the Zeeman frequency ω_S.

Taking the system-environment interaction into account, the effect of the coupling operator $\widehat{\mathcal{H}}_{SE}^L$ is the generation of product terms of the form $\hat{S}_\pm \hat{I}_z^j$ in the density operator, correlating the system with the environment. Since we only observe the system part of the total Hilbert space, we effectively project the correlated system onto this subspace,

$$\hat{\rho}_S = \text{Tr}_I\{\hat{\rho}_{\text{tot}}\}, \tag{7}$$

where Tr_I represents the partial trace over the environmental degrees of freedom and $\hat{\rho}_{\text{tot}}$ represents the density operator of system plus environment. The result of this projection corresponds to a loss of coherence by dephasing. This free evolution of the system under the SE interaction is called the free induction decay (FID) in NMR terminology. The decay process of the system state is usually called relaxation in NMR terminology or decoherence in quantum information.

In the following, we will describe the dynamics of the system in a rotating frame of reference [38]: The system rotates at the (angular) frequency ω_S around the z axis and the environment at ω_I. As a result, the rotating frame Hamiltonian becomes

$$\widehat{\mathcal{H}}_f = \widehat{\mathcal{H}}_S + \widehat{\mathcal{H}}_{SE} + \widehat{\mathcal{H}}_E, \tag{8}$$

where

$$\widehat{\mathcal{H}}_S = \widehat{\mathcal{H}}_S^L - \omega_S \hat{S}_z = \hat{0}, \tag{9}$$

$$\widehat{\mathcal{H}}_{SE} = \hat{S}_z \sum_j b_{Sj} \hat{I}_z^j, \tag{10}$$

$$\widehat{\mathcal{H}}_E = \widehat{\mathcal{H}}_E^L - \omega_I \sum_j \hat{I}_z^j = \sum_{i<j} d_{ij} \left[2\hat{I}_z^i \hat{I}_z^j - \left(\hat{I}_x^i \hat{I}_x^j + \hat{I}_y^i \hat{I}_y^j \right) \right]. \tag{11}$$

This transformation is exact, since the Zeeman terms commute with all other terms in the Hamiltonian as well as with the equilibrium density operator.

The effect of the environment-Hamiltonian $\widehat{\mathcal{H}}_E$ on the evolution of the system may be discussed in an interaction representation with respect to the evolution of the isolated environment: the system-environment Hamiltonian then becomes

$$\widehat{\mathcal{H}}_{\text{SE}}^{(E)}(t) = e^{-i\widehat{\mathcal{H}}_E t} \widehat{\mathcal{H}}_{\text{SE}} e^{i\widehat{\mathcal{H}}_E t}$$
$$= \hat{S}_z e^{-i\widehat{\mathcal{H}}_E t} \left(\sum_j b_{Sj} \hat{I}_z^j \right) e^{i\widehat{\mathcal{H}}_E t}. \quad (12)$$

Since $\widehat{\mathcal{H}}_E$ does not commute with $\widehat{\mathcal{H}}_{\text{SE}}$, the effective system-environment interaction $\widehat{\mathcal{H}}_{\text{SE}}^{(E)}$ becomes time dependent: the system experiences a coupling to the environment that fluctuates. The correlation time τ_B of the time-dependent spin-bath operators $\hat{I}_z^j(t) = e^{-i\widehat{\mathcal{H}}_E t} \hat{I}_z^j e^{i\widehat{\mathcal{H}}_E t}$ is defined by the decay to $1/e$ of the correlation function

$$i_z^j(t) = \frac{\text{Tr}\left\{ \hat{I}_z^j(0) \hat{I}_z^j(t) \right\}}{\text{Tr}\left\{ \hat{I}_z^j(0) \hat{I}_z^j(0) \right\}}. \quad (13)$$

Considering that all the bath spins are equivalent, the latter correlation functions are identical for every j and share the same correlation time τ_B.

III. DYNAMICAL DECOUPLING

A. Notation

The aim of dynamical decoupling is the reduction of the interaction of the qubit system with the environment, thus retaining the quantum information for as long as possible. In the context of DD, it is assumed that it is possible to apply arbitrary single-qubit operations to the system qubit, but that it is not possible to control the environment. One thus applies to the system short, strong pulses, whose effect can be described as a refocusing of the system-environment interaction by the control Hamiltonians $\widehat{\mathcal{H}}_{\text{C(S)}}(t)$ [8,9].

Let us refer to Fig. 1 and consider a single cycle of the sequence having a period τ_c. In the rotating frame, the operator that describes the evolution of the total system from 0 to τ_c is

$$\hat{U}(\tau_c) = \hat{U}_f(\tau_{N+1}) \prod_{i=1}^{N} \hat{U}_C^i(\tau_p) \hat{U}_f(\tau_i), \quad (14)$$

where from Eq. (8) the free evolution operator is

$$\hat{U}_f(t) = \exp\{-i\widehat{\mathcal{H}}_f t\} \quad (15)$$
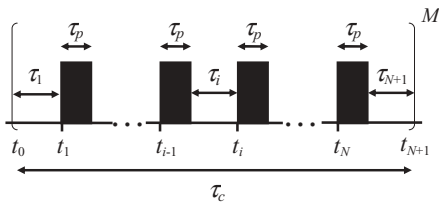

FIG. 1. Schematic representation of dynamical decoupling. The solid boxes represents the control pulses.

and the control evolution operators that act during the time τ_p is

$$\hat{U}_C^i(\tau_p) = T \exp\left\{ -i \int_0^{\tau_p} dt' \left(\widehat{\mathcal{H}}_f + \widehat{\mathcal{H}}_{\text{C(S)}}^i(t') \right) \right\} \quad (16)$$

with T the Dyson time-ordering operator [42,43]. We assume that the free evolution Hamiltonian is constant, while the control Hamiltonian $\widehat{\mathcal{H}}_{\text{C(S)}}^i(t)$ is constant during τ_p but changes for different i. The delay times between the control Hamiltonians are $\tau_i = t_i - (t_{i-1} + \tau_p)$ for $i = 2,..,N+1$ and $\tau_1 = t_1 - t_0$, where $t_0 = 0$, $t_{N+1} = \tau_c$, and t_i represents the time at which the ith control operation starts. Figure 1 shows a graphical representation of these definitions.

Like any unitary evolution, the total propagator can be written as the exponential of a Hermitian operator,

$$\hat{U}(t) = e^{-i\widehat{\mathcal{H}}_{\text{eff}} t}. \quad (17)$$

Using average Hamiltonian theory [16] we can calculate the effective Hamiltonian $\widehat{\mathcal{H}}_{\text{eff}}$ as a series expansion,

$$\widehat{\mathcal{H}}_{\text{eff}} = \widehat{\mathcal{H}}^{(0)} + \widehat{\mathcal{H}}^{(1)} + \widehat{\mathcal{H}}^{(2)} + \cdots = \sum_{n=0}^{\infty} \widehat{\mathcal{H}}^{(n)}. \quad (18)$$

The zero-order term $\widehat{\mathcal{H}}^{(0)}$ is given by the time integral of the total Hamiltonian from time 0 to τ_c. An ideal DD sequence makes $\widehat{\mathcal{H}}^{(0)} = \widehat{\mathcal{H}}_E$, i.e., for ideal pulses, the interaction Hamiltonian vanishes to zeroth order. In the Magnus expansion [44], higher-order terms are proportional to increasing powers of τ_c/τ_B, since we assume that the environment is weakly coupled to the system ($b_{Sj}\tau_B \ll 1$) and in consequence τ_B is the dominant time scale [34].

If the basic cycle is iterated M times (see Fig. 1), the total evolution operator becomes

$$\hat{U}(t = M\tau_c) = [\hat{U}(\tau_c)]^M. \quad (19)$$

B. Ideal and real pulses

The usual approximation of hard pulses having a radio-frequency field $\omega_p \gg b_{Sj}$ and duration $\tau_p \ll d_{i,j}^{-1}, b_{Sj}^{-1}$ implies that we can neglect the free precession Hamiltonian and Eq. (16) simplifies to

$$\hat{U}_C^i(\tau_p) = \exp\{-i\hat{S}_u \theta_p\} \quad (20)$$

in the rotating frame, where $u = x,y,z$ and $\theta_p = \omega_p \tau_p$ is the rotation angle around the u axis. In what follows, we shall denote perfect instantaneous π pulses along x and y by $\hat{X} = \exp\{-i\hat{S}_x\pi\}$ and $\hat{Y} = \exp\{-i\hat{S}_y\pi\}$, respectively, and a free evolution of duration τ by f_τ.

To take the effect of nonideal pulses into account, one needs to consider errors in the axis and angle of rotation. We write the resulting control propagator as the product of the ideal pulse rotation times an error rotation $\exp\{-i\hat{S}_{e_i}\theta_{i,e}\}$:

$$\hat{U}_C^i(\tau_p) = \exp\{-i\hat{S}_{e_i}\theta_{i,e}\} \exp\{-i\hat{S}_{u_i}\theta_p\}. \quad (21)$$

The total evolution operator is thus

$$\hat{U}(\tau_C) = \hat{U}'_{f_{N+1}}(\tau_{N+1}, \tau_p) \prod_{i=1}^{N} \hat{U}_C^i(0) \hat{U}'_{f_i}(\tau_i, \tau_p), \quad (22)$$

where the evolution operators

$$\hat{U}'_{f_i}(\tau_i, \tau_p) = \hat{U}_f(\tau_i) \exp\{-i\hat{S}_{e_i}\theta_{i,e}\} \qquad (23)$$

represent a modified free evolution. Note that $\hat{U}'_{f_1}(\tau_i, \tau_p) = \hat{U}_f(\tau_1)$.

The zero-order average Hamiltonian of the free evolution periods (23) for nonperfect pulses is equivalent to interactions of the general form

$$\widehat{\mathcal{H}}_{SE}^{npp} = a_x\hat{S}_x + a_y\hat{S}_y + a_z\hat{S}_z + \sum_j \left(b_{Sj}^x\hat{S}_x + b_{Sj}^y\hat{S}_y + b_{Sj}^z\hat{S}_z\right)\hat{I}_z^j$$

$$= \sum_{u=x,y,z}\hat{S}_u\sum_j\left(a_u + b_{Sj}^u\hat{I}_z^j\right), \qquad (24)$$

where a_u and b_{Sj}^u give the renormalized offsets and couplings respectively, which include the errors of the control Hamiltonians. This picture can also consider errors of control pulses when τ_p is comparable with the inverse couplings of the free evolution Hamiltonian.

We now discuss some DD schemes that refocus the system-environment interaction. In all these cases, we assume that the system is initially prepared in a coherent superposition of the computational basis states. We will refer to the initial state of the qubit as $\hat{S}_x$, $\hat{S}_y$, or $\hat{S}_z$, as shown in Fig. 2(a).

C. Hahn echo

The Hahn spin-echo experiment [10] is the pioneer dynamical decoupling method and the building block for newer DD proposals. It consists of the application of a π pulse to the S spin along an axis (say y) transverse to the static field B_0 at time
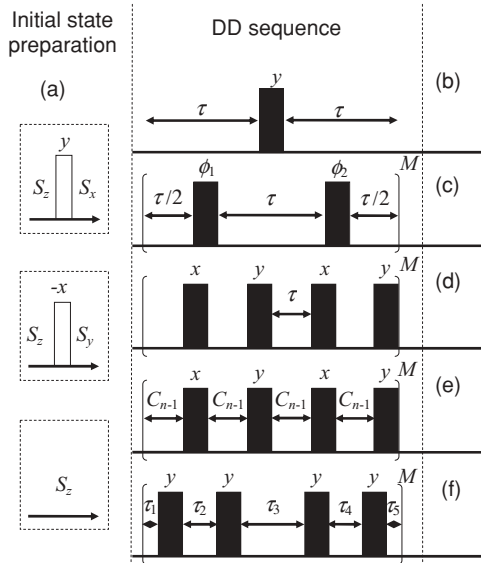

FIG. 2. Schemes of dynamical decoupling pulse sequences. Empty and solid rectangles represent $\pi/2$ and π pulses, respectively. M represents the number of iterations of the cycle. (a) Initial state preparation before application of the DD sequence. (b) Hahn spin-echo sequence. (c) CPMG ($\phi_2 = \phi_1$) and CPMG-2 ($\phi_2 = \phi_1 + \pi$) sequences. (d) PDD sequence. (e) CDD sequence of order n, CDD$_n$ = C_n. (f) UDD sequence scheme with four pulses, i.e., UDD of order 4, UDD$_4$.

τ causing an echo at time 2τ [Fig. 2(b)]. The total evolution operator can be summarized as $f_\tau\hat{Y}f_\tau$ where the total time (assuming a delta-function pulse) is 2τ. As a consequence, the zero-order average Hamiltonian is

$$\widehat{\mathcal{H}}_{Hahn}^{(0)} = \frac{1}{2\tau}\int_0^{2\tau}dt'\widehat{\mathcal{H}}(t') = \frac{(\tau\widehat{\mathcal{H}}_{SE} - \tau\widehat{\mathcal{H}}_{SE})}{2\tau} = 0. \quad (25)$$

The resulting system evolution operator approaches the identity to within $O((\tau_c/\tau_B)^2)$. Thus if $\tau_c \ll \tau_B$, a perfect echo (time reversion) is achieved at the total evolution time $t = 2\tau = \tau_c$. When τ_c is comparable to or longer than τ_B, the echo decays due to the higher order terms.

D. Carr-Purcell and Carr-Purcell-Meiboom-Gill

To avoid the decay of the echo due to the finite correlation time of the environment, Carr and Purcell [11] reduced the cycle time by splitting the total time into shorter segments of equal length and a refocusing pulse in the middle of each segment.

Figure 2(c) shows the pulse sequence for an initial condition of $\hat{S}_x$ with $\phi_1 = \phi_2 = y$. The resulting evolution operator is $f_{\tau/2}\hat{Y}f_\tau\hat{Y}f_{\tau/2}$. Later on, Meiboom and Gill [12] suggested to shift the phase of the refocusing pulses by $\pi/2$, so the rotation axis is the same as the orientation of the initial state. For perfect pulses, both cases are equivalent, but only the CPMG version compensates flip-angle errors of the refocusing pulses. For a flip-angle error $\exp\{-i\hat{S}_{e_i}\theta_{i,e}\} = \exp\{-i\hat{S}_y\Delta\omega_1\tau_p\}$ for every i in Eq. (23), the zero-order average Hamiltonian is proportional to $\Delta\omega_1\hat{S}_y$. It thus commutes with an initial condition along the y axis, (the CPMG case) and has no effect, but it causes an unwanted rotation of an initial state $\propto \hat{S}_x$ (the CP case). In the following we call this sequence with identical π pulses CPMG.

An alternative sequence that also compensates flip-angle errors of the refocusing pulses is shown in Fig. 2(c), with $\phi_2 = \phi_1 + \pi = -y$. For hard pulses and vanishing delays between the pulses, the zero-order average Hamiltonian of this sequence vanishes, for arbitrary flip-angle errors, and the first nonvanishing term is of order τ_c/τ_B and proportional to $\hat{S}_x$. As a consequence, an initial condition proportional to $\hat{S}_x$ is less affected under this sequence. In what follows, we will call this DD sequence CPMG-2.

The effect of pulse errors during CPMG and CPMG-2 on the spin dynamics was studied in Refs. [45–51], and we will show some effects in the following sections.

E. Periodic dynamical decoupling

A sequence called XY-4 in the NMR community was proposed initially to compensate the sensitivity of the CPMG-like sequences to nonperfect pulses [13,14]. Later, it was found equivalent to the shortest universal DD sequence that cancels the zero-order average Hamiltonian for a general SE interaction of the form (24) [34,52]. This sequence, depicted in Fig. 2(d) and called periodic dynamical decoupling (PDD), has an evolution operator of the form $\hat{Y}f_\tau\hat{X}f_\tau\hat{Y}f_\tau\hat{X}f_\tau$. Because it suppresses SE interactions of the form (24), it compensates errors of nonideal pulses at the end of the cycle.

F. Concatenated dynamical decoupling

The CDD scheme [17,34] recursively concatenates lower-order sequences to effectively increase the decoupling order. The CDD evolution operator for a recursion order of n is given by

$$\text{CDD}_n = C_n = \hat{Y}C_{n-1}\hat{X}C_{n-1}\hat{Y}C_{n-1}\hat{X}C_{n-1}, \quad (26)$$

where $C_0 = f_\tau$ and $\text{CDD}_1 = \text{PDD}$. Figure 2(e) shows a general scheme for this process. Each level of concatenation reduces the norm of the first nonvanishing order term of the Magnus expansion of the previous level, provided that the norm was small enough to begin with. The latter reduction is at the expense of an extension of the cycle time by a factor of four.

G. Uhrig dynamical decoupling (UDD)

Uhrig proposed a different approach to the goal of keeping a qubit alive [20,53]: For a given number N of pulses during a total time τ_c, at what times should these pulses be applied to minimize the effect of the system-environment interaction? The solution he found for the times t_i is

$$t_i = \tau_c \sin^2\left[\frac{\pi i}{2(N+1)}\right], \quad (27)$$

where $t_{N+1} = \tau_c$ is the cycle time and $t_0 = 0$ the starting time. Defining $\tau_i = t_i - t_{i-1}$ the UDD evolution operator for a sequence of N pulses is

$$\text{UDD}_N = f_{\tau_{N+1}}\hat{Y}f_{\tau_N}\hat{Y}\cdots\hat{Y}f_{\tau_2}\hat{Y}f_{\tau_1} \quad (28)$$

and its schematic representation is given in Fig. 2(f). The CPMG sequence is the simplest UDD sequence of order $N = 2$.

Cywinski *et al.* explained the performance of the DD sequence by finding its spectral filter for the bath modes [54]. They found that the effect of the UDD pulse sequence leads to an efficient spectral filter for slow motion bath modes. It was shown that UDD is the best sequence for reducing the SE interaction in the limit of low-frequency noise [20,53,54]. Rigorous performance bounds for the UDD sequence were found by Uhrig and Lidar in Ref. [55].

IV. EXPERIMENTAL RESULTS

A. System and environment

Experiments were performed on a polycrystalline adamantane sample using a home-built solid-state NMR spectrometer with a ^{1}H resonance frequency of 300 MHz. The adamantane molecule contains two nonequivalent carbon atoms. Under our conditions, they have similar dynamics. Working with natural abundance (1.1%), the interaction between the ^{13}C-nuclear spins can be neglected. The main mechanism for decoherence is the interaction with the proton spins. As discussed in Sec. II, this interaction (12) is not static, since the dipole-dipole couplings within the proton bath cause flip-flops of the protons coupled to the carbon.

Considering that all the proton spins I are equivalent, we can estimate the correlation time of the time-dependent SE interaction (12) with the decay time of the correlation function
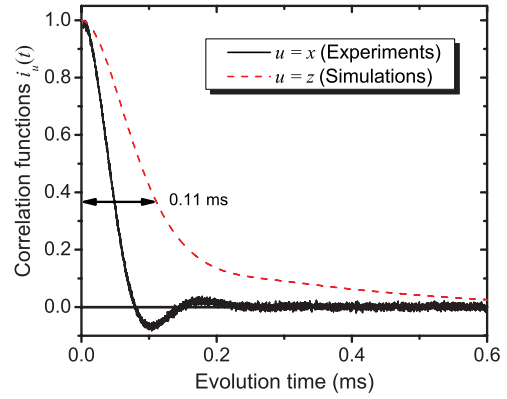

FIG. 3. (Color online) Evolution of the normalized spin correlation functions for the bath spins (protons). The solid line represents the proton FID signal $[i_x(t)]$ and the dashed line the numerically simulated $i_z(t)$.

$i_z^j(t)$. While the correlation functions $i_z^j(t)$ of Eq. (13) cannot be measured directly because we cannot address individual spins of the bath, we get a very good estimate by measuring

$$i_x(t) = \frac{\text{Tr}\{\hat{I}_x(0)\hat{I}_x(t)\}}{\text{Tr}\{\hat{I}_x(0)\hat{I}_x(0)\}}, \quad (29)$$

i.e., the proton free-induction decay (FID) (solid line in Fig. 3). The time evolutions in equation (29) are determined by the bath Hamiltonian $\widehat{\mathcal{H}}_E$, $\hat{I}_x(t) = e^{-i\widehat{\mathcal{H}}_E t}\hat{I}_x e^{i\widehat{\mathcal{H}}_E t}$ and $\hat{I}_x = \sum_j \hat{I}_x^j$. Simulating it with the dipole-dipole Hamiltonian of Eq. (11) and using the same Hamiltonian for calculating $i_z^j(t)$, we find the correlation function represented with dashed line in Fig. 3. The spectral density of the bath is well approximated by a normal (Gaussian) distribution and the system-environment interaction is weak compared with the intrabath interaction ($|b_{Sj}|\tau_B \lesssim 1/3$).

The π pulses for DD were applied on resonance with the ^{13}C spins. Their radiofrequency (rf) field of $2\pi \times 48$ kHz gives a π-pulse length of $\tau_p = 10.4$ μs. The measured rf field inhomogeneity is about 10%. We performed experiments where the delay τ between successive DD pulses was varied from 10 to 200 μs. We prepared the initial state by using the sequences of Fig. 2(a) and we measured the survival probability of the magnetization

$$s_u(t) = \frac{\text{Tr}\{\hat{S}_u(0)\hat{S}_u(t)\}}{\text{Tr}\{\hat{S}_u(0)\hat{S}_u(0)\}}, \quad (30)$$

where $u = x,y,z$. The solid line of Fig. 4 shows the experimental observation of this survival probability from an initial condition $\hat{S}_x$ under a free evolution (^{13}C FID).

B. Hahn echo

As shown in Fig. 4, the decay of the S-spin magnetization is reduced by the Hahn-echo sequence. The results of the Hahn echo are marked by square points. Compared to the free induction decay, the decay rate is reduced approximately by a factor of 2.
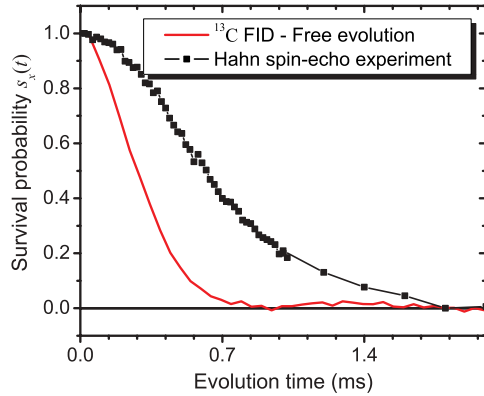
FIG. 4. (Color online) Survival probability of the S-spin under free evolution (^{13}C FID) and after a Hahn-echo sequence. An initial condition $\hat{S}_x$ was prepared.

C. CPMG

Figure 5 shows the experimental results of the CPMG sequence of Fig. 2(c) with $\phi_1 = \phi_2 = y$. Different rows correspond to different initial conditions $\hat{S}_x$, $\hat{S}_y$, and $\hat{S}_z$ of the ^{13}C qubit. The left-hand panels show the survival probability (30) as a function of the total evolution time $t = M\tau_c$ (including the pulses), and the right-hand panels show the same data as a function of the number of applied pulses.
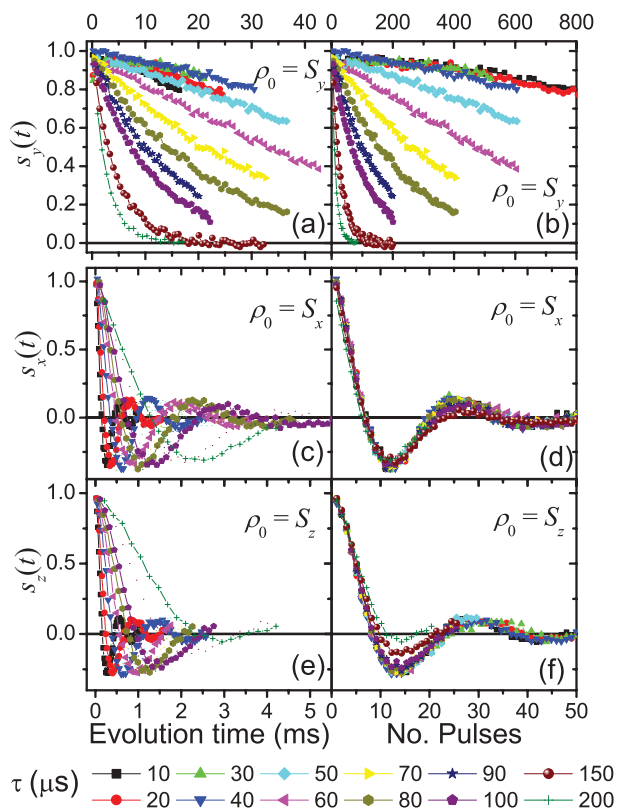
FIG. 5. (Color online) Magnetization evolution for the CPMG sequence. From top to bottom the initial conditions are $\hat{S}_y$, $\hat{S}_x$, and $\hat{S}_z$. The left-hand panels represent the ^{13}C magnetization as a function of the total evolution time while right-hand panels show its evolution as a function of the number of applied pulses. The legend at the bottom gives the delays τ between successive pulses.

The plots show that the decay of the survival probability depends crucially on the initial state of the qubit; we shall henceforth refer to the initial state in the direction of the DD pulses as the "longitudinal" state and the ones perpendicular to the pulses as the "transverse" states. Flip-angle errors, which arise from inhomogeneous radiofrequency fields, are usually the dominant imperfection in this type of experiments. When the CPMG sequence is applied to a longitudinal initial condition, flip-angle errors do not affect the performance of the decoupling, since they are compensated over each cycle consisting of two pulses [12]. As a result, the decay rates for longitudinal states are about an order of magnitude lower than for transverse initial conditions. We also observe an unexpected oscillation pattern for transverse initial states. These kind of strong asymmetries have been reported in different samples and have been hypothesized to be due to stimulated echoes induced by pulse errors [45,47,50,51] or due to the non-negligible effects of the interaction Hamiltonian acting during the finite width pulses [46,48,49].

The right-hand panels show the same data but plotted against the number of pulses. They clearly show that the oscillation frequency depends on the number of applied pulses or equivalently on the total pulse-irradiation time. Similar oscillations have been also reported in different samples [46,48–50]. In our experiments, the oscillation pattern originates from the bimodal distribution of rf field amplitudes in the coil. For our present analysis, the beating is not important because it could be reversed [49] or avoided by improving the rf field coil. We instead concentrate on the decay of the envelope, which represents the overall survival probability of the signal.

For the longitudinal initial state (upper panel), Fig. 5(b) shows that the signal decay, as a function of the distance τ between successive pulses, remains constant until $\tau = 30$ μs. The corresponding cycle time is $\tau_c = 2\tau + 2\tau_p = 80.8$ μs, which is comparable to the bath correlation time τ_B; hence; the signal decay for cases below $\tau = 30$ μs is mainly due to pulse errors. For longer delays $\tau_c > \tau_B$ ($\tau_B \sim 110$ μs), the decay rate increases because of the reduction of time reversal efficiency in the fluctuating environment.

D. CPMG-2

Figure 6 shows the corresponding results for the CPMG-2 sequence. Since the first nonvanishing order of the Magnus expansion for the CPMG-2 sequence (considering flip-angle errors) commutes with $\hat{S}_x$, we expect that the signal decay for the $\hat{S}_x$ initial state is similar to that of the longitudinal initial state of the CPMG experiments. The experimental results shown in Fig. 6 clearly agree with this expectation. For the other initial states, an oscillatory behavior similar to that for the transverse state of the CPMG is observed. Although the oscillation still depends on the number of pulses (right panels), the frequency is slower than in the CPMG case, and the envelope of the oscillations decays more slowly. The origin of the oscillation pattern is again the bimodal distribution of the inhomogeneity of the rf field generating an effective field along the x axis. The experimentally observed oscillation agrees with the results of the effective nutation experiment. Again, we will concentrate on the decay of the envelope.
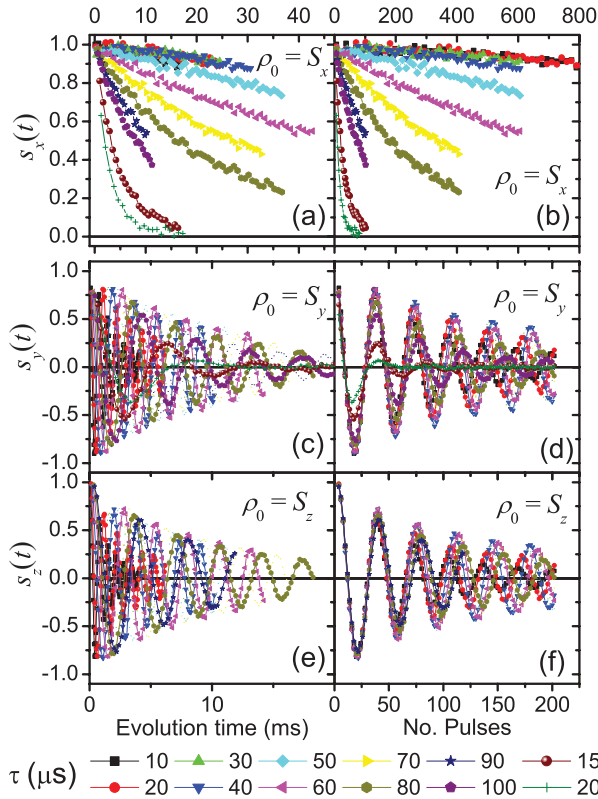
FIG. 6. (Color online) Magnetization evolution for the CPMG-2 sequence. From top to bottom the initial conditions are $\hat{S}_x$, $\hat{S}_y$, and $\hat{S}_z$. The left-hand panels represent the ^{13}C magnetization as a function of the total evolution time, while the right-hand panels show its evolution as a function of the number of applied pulses. The legend at the bottom gives the delays τ between successive pulses.
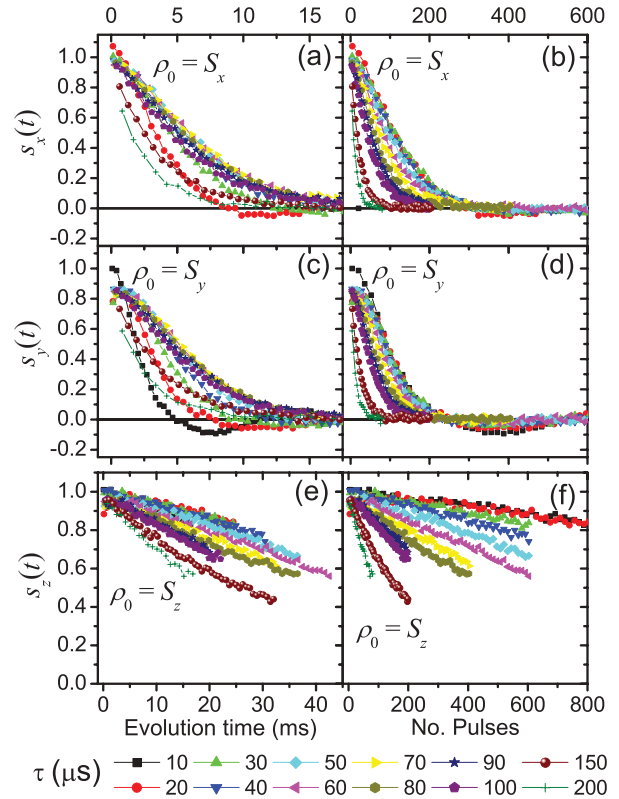
FIG. 7. (Color online) Signal decay of the initial state of the qubit for the PDD sequence. From top to bottom the initial conditions are $\hat{S}_x$, $\hat{S}_y$, and $\hat{S}_z$. The left-hand panels represent the decay as a function of the total evolution time while the right-hand panels show the decay as a function of the number of applied pulses. The legend at the bottom gives the delays τ between successive pulses.

E. PDD

Figure 7 shows the signal decay for different initial conditions under the application of the PDD sequence of Fig. 2(d). One observes that the signal decay evolves qualitatively similar for initial conditions in the plane transverse to the static field, i.e., $\hat{S}_x$ and $\hat{S}_y$. This agrees with the theoretical predictions: The sequence of evolutions $\hat{Y} f_\tau \hat{X} f_\tau \hat{Y} f_\tau \hat{X} f_\tau$ is nearly symmetric with respect to x vs. y. The decays still contain a small oscillatory contribution. Since it appears to depend mostly on the number of pulses, rather than on the delays between them, we attribute them to pulse errors that are not completely canceled. Compared to CPMG and CPMG-2, the period of the oscillation is one order of magnitude longer, indicating that the effect of the pulse imperfections has been reduced by an order of magnitude. This general improvement against pulse errors is because the sequence cancels the zeroth-order average Hamiltonian of the more general SE interaction (24), while the CPMG sequences cancel only its pure-dephasing part.

In Figs. 7(b) and 7(d), the decay rates, in units of pulses, up to $\tau = 40$ μs, i.e., $\tau_c = 4(\tau + \tau_p) = 201.6$ μs, are equal to within experimental error. This shows that the sequence is more robust, compared to previous sequences, in the regime where τ_c exceeds the bath-correlation time. However, from the time evolution of Figs. 7(a) and 7(c), the decay rate is larger than the longitudinal case of CPMG or the $\hat{S}_x$ case of CPMG-2.

If the initial state is proportional to $\hat{S}_z$, its evolution is qualitatively different. We believe that this results from the fact that it is parallel to the static field and commutes with the free precession Hamiltonian (8). As a consequence, this evolution reflects the implementation errors of the sequence. The source of the decay is the pulse errors due to which the average Hamiltonian no longer commutes with the initial state. This experiment provides a means of quantifying pulse errors, and calibrating an optimal setup of the sequence to enhance its performance.

F. CDD

The qualitative behavior of the CDD experiments is similar between different orders and to the PDD one, but they change in the time scale for which the initial state can be maintained. They are also more robust against pulse errors—the oscillation pattern is not observed. For details of the survival probability evolution see Appendix. A summary of the results is presented in Fig. 8 in Sec. V where the decay times for different CDD orders and delays τ between pulses are plotted.

G. UDD

The experimental survival probabilities for the UDD sequences have the same qualitative behavior as the CPMG curves. They manifest the same asymmetries with respect to the initial state. That is expected because UDD sequences also
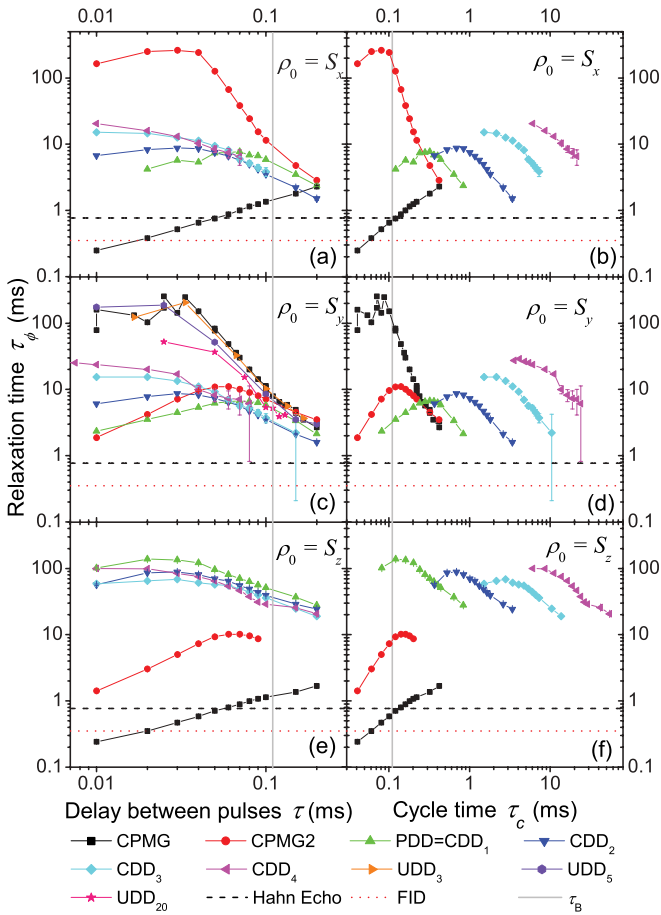
FIG. 8. (Color online) Relaxation times of different initial conditions under DD conditions as a function of the delay between pulses τ (left panels) and the cycle time τ_c (right panels). From top to bottom the initial condition is given by $\hat{\rho}_0 = \hat{S}_x$, $\hat{S}_y$, and $\hat{S}_z$ respectively. An optimal τ and consequently τ_c is observed for each sequence. The reduction of the relaxation time to the right side of the optimal value is due to the shifting environment: in this regime the cycle time is longer than the correlation time of the bath, $\tau_c > \tau_B$. The reduction for short cycle times indicates that in this regime, accumulated pulse errors dominate.

only reduce SE interactions of the form (10). We observed that with increasing UDD order, the decay rates increase, as predicted in Ref. [55] for the conditions satisfied in our experiments where $|b_{Sj}|\tau_B < 1$ and $\tau_c \sim \tau_B$. A summary of the rates is shown in the next section in Fig. 8 where we have used τ as the average delay between pulses. An extensive analysis of the performance of UDD sequences and nonequidistant pulse sequences against equidistant ones for the present experimental conditions will be given elsewhere [56].

V. COMPARISONS: OPTIMAL CHOICES

The goal of DD is the preservation of quantum states by the application of suitable decoupling sequences. If the pulses are ideal and they are applied with very short delays, it is possible to preserve quantum states for arbitrarily long times in the presence of a system-environment coupling that is linear in the system operators. However, for experiments using nonideal pulses, a finite cycle time optimizes the DD performance. This

can be seen very clearly in the summary of the experimental results presented in Fig. 8. The left panels show the DD decay times as a function of the delay τ for every sequence and different initial conditions. As an example, for CPMG when the initial condition is longitudinal to the pulses ($\hat{S}_y$), the optimal cycle time is $\tau_c = 80.8\,\mu s$ ($\tau = 30\,\mu s$). For longer cycle times, the decay time gets shorter, since the environment changes during the cycle and the refocusing efficiency decreases.

While shorter cycle times should give even better results under ideal conditions, we find experimentally a decrease of the relaxation time. This can be attributed to an accumulation of pulse errors, which dominates in this regime. Similar results are observed for the CPMG-2 if we exchange $\hat{S}_y$ with $\hat{S}_x$. This can be seen clearly under conditions of transverse initial states ($\hat{S}_x$ for CPMG) where the decay time is proportional to the cycle time. This means that the error per cycle is independent of the cycle time and corresponds thus to a zero-order term of the average Hamiltonian. This is the behavior expected for flip angle errors, which are the main source of the decay in this regime. Since flip angle errors are in no way compensated for transverse states in the CPMG sequence, their accumulated effect is so strong that the optimal cycle time exceeds τ_B and the sequence performs only marginally better than the Hahn-echo sequence, which has the longest cycle time.

If we consider the CPMG-2 sequence with the initial conditions $\hat{S}_y$ and $\hat{S}_z$, the decay time grows $\propto \tau_c^2$ for short times. This implies that in this case, the dominant error term is proportional to τ_c, i.e., it corresponds to a first-order term of the average Hamiltonian. Moreover, its optimal relaxation time is one order of magnitude longer than the Hahn-echo decay time.

The behavior of the UDD sequences is similar to that of CPMG. We show here only their decay times for $\hat{S}_y$ as initial condition [Fig. 8(c)], i.e., longitudinal to the DD pulses. They are plotted as a function of the average delay between pulses. The figure shows that the UDD decay times are always shorter than those of CPMG. Moreover, increasing the UDD order reduces the decay time, as expected by theoretical expectations when $|b_{Sj}|\tau_B < 1$ and $\tau_c \sim \tau_B$ [55]. A regime where UDD performs better than CPMG may perhaps exist at short cycle times compared with τ_B [56], provided the pulse errors can be made sufficiently small that they do not dominate over external sources of decoherence. Recent proposals of UDD based sequences that reduce decoherence of a general SE interaction, like Eq. (24), could allow one to find this regime [21,22].

For PDD the optimal cycle time for $\hat{S}_x$ and $\hat{S}_y$ is $\tau_c = 321.6\,\mu s$, ($\tau = 70\,\mu s$), which is longer than τ_B. The resulting performance is relatively poor. The resulting decay time is similar to that of CPMG for the same cycle time [Fig. 8(d)] or CPMG-2 for the $\hat{S}_x$ initial condition [Fig. 8(b)]. However, for these particular initial conditions CPMG and CPMG-2 can be made to perform an order of magnitude better by reducing the cycle time.

For CDD$_2$ with initial conditions transverse to the static field, the optimal cycle time is $\tau_c = 16\tau + 20\tau_p = 688\,\mu s$, i.e., $\tau = 30\,\mu s$. For CDD$_3$ and CDD$_4$ the shortest delay time between pulses of $\tau = 10\,\mu s$ and $\tau = 2.5\,\mu s$ are the optimal situations, giving $\tau_c(CDD_3) = 64\tau + 84\tau_p = 1513.6\,\mu s$ and $\tau_c(CDD_4) = 256\tau + 388\tau_p = 4675.2\,\mu s$. The optimal delay τ becomes shorter with increasing CDD order, because the cycle time increases by a factor of 4 for each level of concatenation.
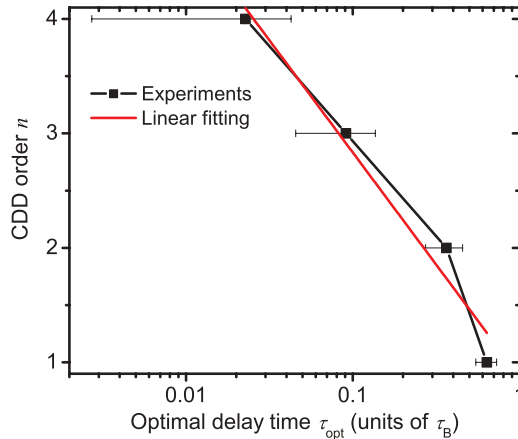
FIG. 9. (Color online) CDD order n as a function of its optimal delay between pulses τ_{opt} to reduce decoherence. The experimental square points seem to satisfy a relation given by $n = c - b \ln(\tau_{\text{opt}}/\tau_B)$. The solid (red) line shows a fitting curve with parameters $c = (0.9 \pm 0.2)$ and $b = (-0.9 \pm 0.1)$.

Apparently, the pulse errors do not accumulate as strongly as in the case of CPMG, which may be attributed to the fact that CDD is designed to compensate pulse errors [17,34]. The crossover cycle time, where the transition occurs from a decay dominated by pulse errors to the regime where the decay is dominated by the short bath correlation time is increased, as shown in the right-hand panels. Even for cycle times that are much longer than the bath-correlation time, the CDD provides a significant reduction of the decoherence rate compared to the free evolution decay (dotted lines) and the Hahn-echo decay (dashed lines). An optimal cycle time when considering imperfect finite pulses was predicted by Khodjasteh and Lidar [34]. Figure 9 shows the experimental relation between the optimal delays τ and their respective CDD order n (square points). It seems to satisfy a relation given by $n = c - b \ln(\tau_{\text{opt}}/\tau_B)$, where c and b are constants and τ_{opt} is the optimal delay for a given n (see below).

The unifying result of the curves shown in the left-hand panels of Fig. 8 is that the optimal delay between pulses is always shorter than the bath correlation time, with comparable values for all sequences, with the single exception of the CPMG sequence for initial conditions $\hat{S}_x$ and $\hat{S}_z$, as discussed above. Clearly, this time scale is determined by the (average) delay between pulses τ, not by the cycle time τ_c. Expressing this differently, one might say that only a small fraction of what is lost in a single echo can be refocused by compensated sequences. If we look at pulse spacings longer than the bath correlation time τ_B, the differences between sequences become very small and the decay times approximate those of FID and Hahn echo. Accordingly, it appears important to keep the number of pulses per unit time constant when comparing different DD sequences.

We now compare the different DD sequences with the optimal delay between pulses for each sequence. Figure 10 shows the evolution of the survival probabilities for different initial conditions for all the sequences discussed here.

As a general rule, we note that for increasing CDD order, the optimal pulse delay τ gets shorter and for longer delays
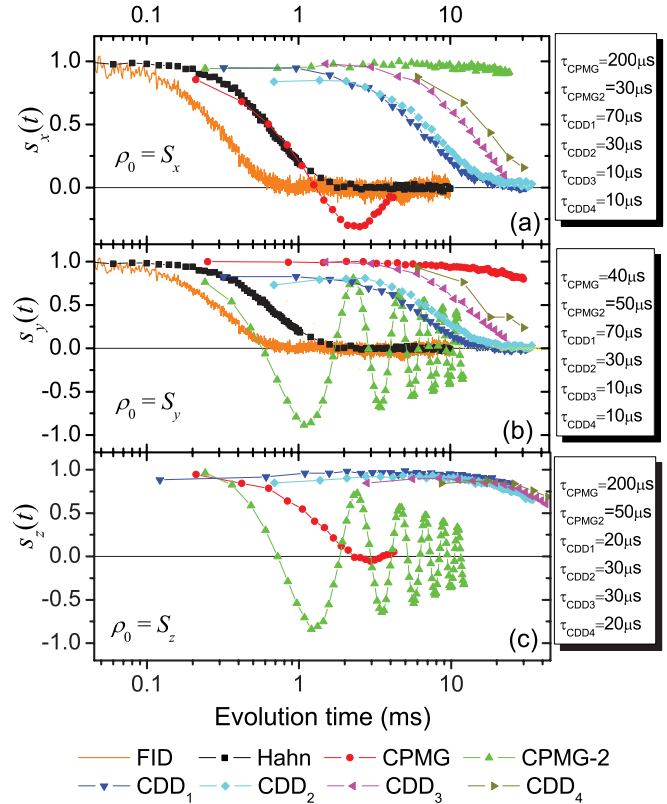

FIG. 10. (Color online) Time evolution of the survival probability for the optimal delay between pulses of the different DD sequences. From top to bottom the initial states are $\hat{S}_x$, $\hat{S}_y$, and $\hat{S}_z$. The optimal delays τ are given in the legends.

between pulses, higher CDD orders do not perform better than lower CDD orders. Hence, keeping the delay between pulses constant, there is an optimal CDD order for reducing decoherence as predicted in Refs. [34,35]. It is difficult to find accurately the optimal CDD order as a function of τ from Figs. 8(a) and 8(c) in order to compare with the theoretical predictions of Eq. (140) in Ref. [35]. However, the relation given in Fig. 9 for the optimal delay between pulses τ_{opt} behaves similar. A linear fitting of the experimental data gives $n = c - b \ln(\tau_{\text{opt}}/\tau_B)$ with $c = (0.9 \pm 0.2)$ and $b = (-0.9 \pm 0.1)$ agreeing well with the predicted expression [35].

The best DD sequence and its corresponding optimal cycle time depends on hardware limitations and importantly on the desired goal. If one aims to freeze a quantum state during a short time, its value will bound the cycle time and as a result, the maximal CDD order that can be applied. For longer times, increasing the CDD order will be advantageous, but power dissipation may force a reduction in the number of pulses and simultaneously the CDD order. For specific initial conditions, CPMG and CPMG-2 are the best choices for reducing decoherence; however, the large asymmetry of these sequences to other initial conditions limits their usefulness when the initial state of the qubit is unknown. Note that in these cases, it has been shown that coherences could be frozen as labeled polarization [51]. If the goal is the preservation of an unknown quantum state, the CDD sequences provide the best overall performance.

While the SE interaction produces pure dephasing to the spin, in principle DD sequences that compensate pure dephasing decoherence should be sufficient. In consequence concatenating sequences like $f_\tau \hat{Y} f_\tau \hat{Y}$, which reduce pure dephasing processes, could be beneficial. However, the finite precision of control pulses generates an effective Hamiltonian of the form (24), and thus sequences developed to reduce pure dephasing processes have asymmetric performances against initial states directions, i.e., they do not generate a unit evolution operator of the qubit. Thus, we compared, as a test bed, CPMG/UDD sequence that compensate pure dephasing with XY-4 [13,14] based sequences that compensate a general interaction in order to show their effects against pulse errors.

From our results it is evident that for short delays the main source of DD decays are static pulse errors; this limits the maximal performance. However, CPMG and CPMG-2 show the potentially achievable DD performance if the pulse errors are reduced. This implies that new DD proposals should focus on the compensation of pulse errors for these kinds of experimental conditions, similar to the proposal by Viola and Knill [15] or Uhrig and Pasini [57,58]. CDD-type sequences do compensate for pulse errors but only at the end of the CDD cycle. This limits their performance because of the exponential growth of the cycle time with the CDD order. As an alternative method, we suggest to find sequences that compensate pulse errors to zero order during each step of the concatenation procedure. That would be advantageous because the zero-order compensation cycle time remains constant and equal to the PDD cycle time, as assumed for ideal pulses.

VI. CONCLUSIONS

We have experimentally applied different dynamical decoupling sequences to a qubit-system coupled to a spin-bath in order to test and compare their performance. The system used is typical for spin-based solid-state systems where the spectral density of the bath is given by a normal (Gaussian) distribution and the system-environment interaction is weak compared with the intrabath interaction. The experiments were performed in the regime where the average spacing between the pulses is comparable to the bath-correlation time. This article focuses on measuring and fighting decoherence, and the results do not depend on the readout or initialization scheme used for that purpose. Thus, the results should apply directly to other spin-based quantum information processing systems, such as electron spins in diamonds [30–32], electron spins in quantum dots [28,29,39], and donors in silicon [40,41].

While the design of DD sequences is typically based on the assumption that the cycle times is shorter than the bath-correlation time, we demonstrated that even without satisfying this condition, dynamical decoupling reduces decoherence significantly. We showed that the main limitation to the reduction of the DD decay rates is due to the finite precision of the control operations: In our system, flip-angle errors were the main source. Therefore, CPMG or UDD-type sequences that reduce purely dephasing or purely dissipative interactions with the bath perform well only for specific initial conditions of the qubit ensemble. For the privileged initial condition,

CPMG-type sequences performed better than any other DD sequence. But, if the goal is to approach a unit evolution operator, PDD sequence and its concatenated form (CDD) are the best overall option. In agreement with previous predictions [34–36] our results show that, depending on limitations of hardware and the required time to keep the initial state coherent, increasing the CDD order is not always useful. There is an optimal CDD order depending on the power available for the control pulses and their finite precision. We present strong evidence that in order to improve dynamical decoupling sequences, they should be designed to compensate pulse errors.

APPENDIX: CDD EXPERIMENTS

Figures 11, 12, and 13 show the experimentally observed signal decays for CDD_2, CDD_3, and CDD_4 respectively.
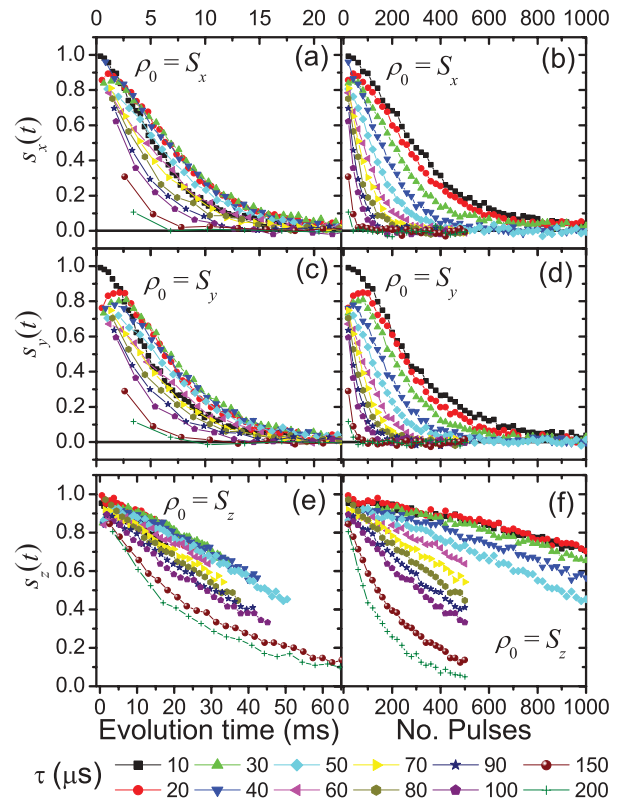

FIG. 11. (Color online) Signal decay of the initial state of the qubit for the CDD_2 sequence. From top to bottom the initial conditions are $\hat{S}_x$, $\hat{S}_y$, and $\hat{S}_z$. The left-hand panels represent the decay as a function of the total evolution time while the right-hand panels show the decay as a function of the number of applied pulses. The legend at the bottom gives the delays τ between successive pulses.
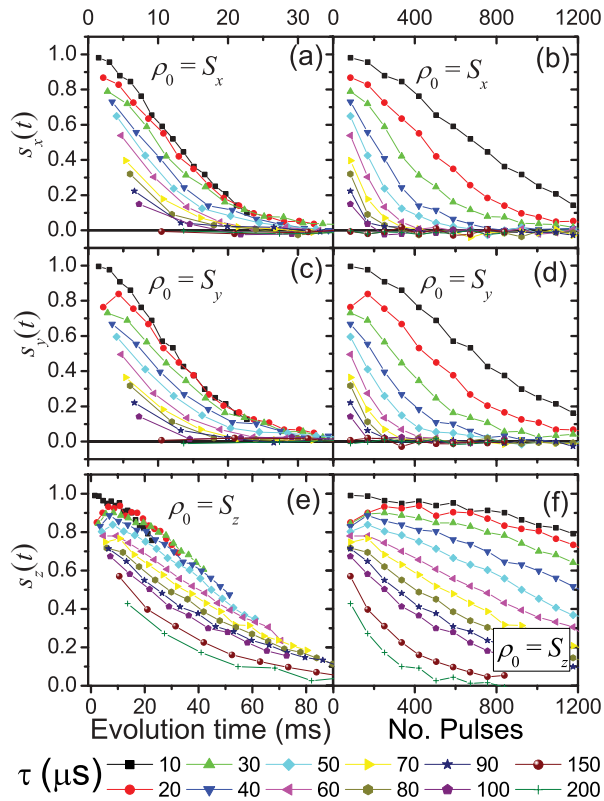
FIG. 12. (Color online) Signal decay of the initial state of the qubit for the CDD_3 sequence. From top to bottom the initial conditions are $\hat{S}_x$, $\hat{S}_y$, and $\hat{S}_z$. The left-hand panels represent the decay as a function of the total evolution time while right-hand panels the decay as a function of the number of applied pulses. The legend at the bottom gives the delays τ between successive pulses.
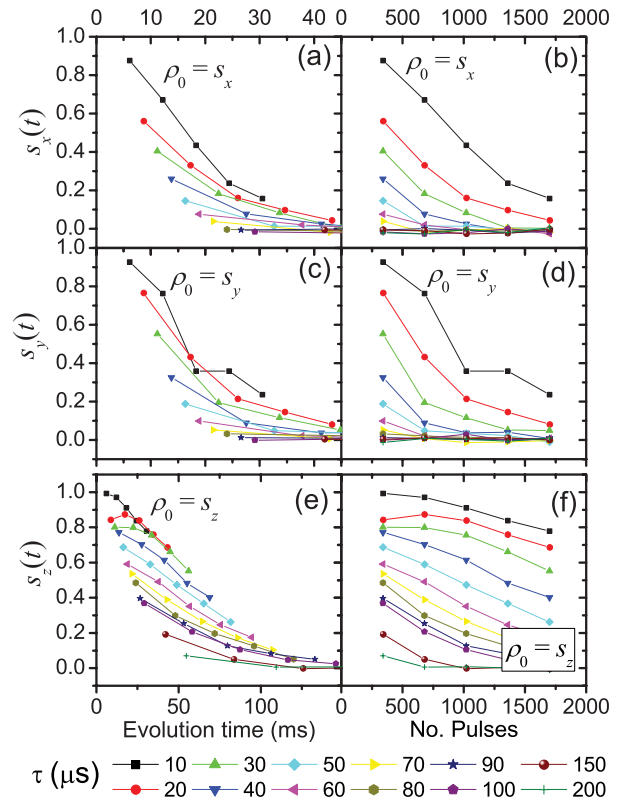
FIG. 13. (Color online) Signal decay of the initial state of the qubit for the CDD_4 sequence. From top to bottom the initial conditions are $\hat{S}_x$, $\hat{S}_y$, and $\hat{S}_z$. The left-hand panels represent the decay as a function of the total evolution time while the right-hand panels show the decay as a function of the number of applied pulses. The legend at the bottom gives the delays τ between successive pulses.

[1] M. A. Nielsen and I. L. Chuang, *Quantum Computation and Quantum Information* (Cambridge University Press, Cambridge, 2000).

[2] W. Zurek, Rev. Mod. Phys. **75**, 715 (2003).

[3] G. DeChiara, D. Rossini, S. Montangero, and R. Fazio, Phys. Rev. A **72**, 012323 (2005).

[4] J. Allcock and N. Linden, Phys. Rev. Lett. **102**, 110501 (2009).

[5] G. A. Álvarez and D. Suter, Phys. Rev. Lett. **104**, 230403 (2010).

[6] J. Preskill, P. Roy. Soc. Lond. A Mat. **454**, 385 (1998).

[7] E. Knill, Nature **434**, 39 (2005).

[8] L. Viola, E. Knill, and S. Lloyd, Phys. Rev. Lett. **82**, 2417 (1999).

[9] W. Yang, Z. Wang, and R. Liu, e-print arXiv:1007.0623.

[10] E. L. Hahn, Phys. Rev. **80**, 580 (1950).

[11] H. Y. Carr and E. M. Purcell, Phys. Rev. **94**, 630 (1954).

[12] S. Meiboom and D. Gill, Rev. Sci. Instrum. **29**, 688 (1958).

[13] A. A. Maudsley, J. Magn. Reson. **69**, 488 (1986).

[14] T. Gullion, D. B. Baker, and M. S. Conradi, J. Magn. Reson. **89**, 479 (1990).

[15] L. Viola and E. Knill, Phys. Rev. Lett. **90**, 037901 (2003).

[16] U. Haeberlen, *High Resolution NMR in Solids: Selective Averaging* (Academic Press, New York, 1976).

[17] K. Khodjasteh and D. A. Lidar, Phys. Rev. Lett. **95**, 180501 (2005).

[18] W. Yang and R. B. Liu, Phys. Rev. Lett. **101**, 180403 (2008).

[19] B. Lee, W. M. Witzel, and S. DasSarma, Phys. Rev. Lett. **100**, 160505 (2008).

[20] G. S. Uhrig, Phys. Rev. Lett. **98**, 100504 (2007).

[21] G. S. Uhrig, Phys. Rev. Lett. **102**, 120502 (2009).

[22] J. R. West, B. H. Fong, and D. A. Lidar, Phys. Rev. Lett. **104**, 130501 (2010).

[23] M. J. Biercuk, H. Uys, A. P. VanDevender, N. Shiga, W. M. Itano, and J. J. Bollinger, Nature **458**, 996 (2009).

[24] M. J. Biercuk, H. Uys, A. P. VanDevender, N. Shiga, W. M. Itano, and J. J. Bollinger, Phys. Rev. A **79**, 062324 (2009).

[25] J. Du, X. Rong, N. Zhao, Y. Wang, J. Yang, and R. B. Liu, Nature **461**, 1265 (2009).

[26] E. R. Jenista, A. M. Stokes, R. T. Branca, and W. S. Warren, J. Chem. Phys. **131**, 204510 (2009).

[27] J. R. West, D. A. Lidar, B. H. Fong, M. F. Gyure, X. Peng, and D. Suter, e-print arXiv:0911.2398.

[28] H. Bluhm, S. Foletti, I. Neder, M. Rudner, D. Mahalu, V. Umansky, and A. Yacoby, e-print arXiv:1005.2995.

[29] C. Barthel, J. Medford, C. M. Marcus, M. P. Hanson, and A. C. Gossard, e-print arXiv:1007.4255.

[30] B. Naydenov, F. Dolde, L. T. Hall, C. Shin, H. Fedder, L. C. L. Hollenberg, F. Jelezko, and J. Wrachtrup, e-print arXiv:1008.1953.

[31] G. de Lange, Z. H. Wang, D. Ristè, V. V. Dobrovitski, and R. Hanson, Science **330**, 60 (2010).

[32] C. A. Ryan, J. S. Hodges, and D. G. Cory, e-print arXiv:1008.2197.

[33] G. Gordon, G. Kurizki, and D. A. Lidar, Phys. Rev. Lett. **101**, 010403 (2008).

[34] K. Khodjasteh and D. A. Lidar, Phys. Rev. A **75**, 062310 (2007).

[35] H. K. Ng, D. A. Lidar, and J. Preskill, e-print arXiv:0911.3202.

[36] T. E. Hodgson, L. Viola, and I. D'Amico, Phys. Rev. A **81**, 062321 (2010).

[37] L. P. Pryadko and G. Quiroz, Phys. Rev. A **80**, 042317 (2009).

[38] A. Abragam, *Principles of Nuclear Magnetism* (Oxford University Press, London, 1961).

[39] R. Hanson, L. P. Kouwenhoven, J. R. Petta, S. Tarucha, and L. M. K. Vandersypen, Rev. Mod. Phys. **79**, 1217 (2007).

[40] B. E. Kane, Nature **393**, 133 (1998).

[41] J. J. L. Morton, A. M. Tyryshkin, R. M. Brown, S. Shankar, B. W. Lovett, A. Ardavan, T. Schenkel, E. E. Haller, J. W. Ager, and S. A. Lyon, Nature **455**, 1085 (2008).

[42] F. Dyson, Phys. Rev. **75**, 486 (1949).

[43] F. Dyson, Phys. Rev. **75**, 1736 (1949).

[44] W. Magnus, Commun. Pure Appl. Math. **7**, 649 (1954).

[45] M. B. Franzoni and P. R. Levstein, Phys. Rev. B **72**, 235410 (2005).

[46] D. Li, A. E. Dementyev, Y. Dong, R. G. Ramos, and S. E. Barrett, Phys. Rev. Lett. **98**, 190401 (2007).

[47] M. B. Franzoni, P. R. Levstein, J. Raya, and J. Hirschinger, Phys. Rev. B **78**, 115407 (2008).

[48] D. Li, Y. Dong, R. G. Ramos, J. D. Murray, K. MacLean, A. E. Dementyev, and S. E. Barrett, Phys. Rev. B **77**, 214306 (2008).

[49] Y. Dong, R. G. Ramos, D. Li, and S. E. Barrett, Phys. Rev. Lett. **100**, 247601 (2008).

[50] M. B. Franzoni, Ph.D. thesis, Universidad Nacional de Cordoba (2010), [http://www.famaf.unc.edu.ar/publicaciones/documents/serie_d/DFis139.pdf].

[51] M. B. Franzoni, R. H. Acosta, and P. R. Levstein, e-print arXiv:1009.0042.

[52] L. Viola and S. Lloyd, Phys. Rev. A **58**, 2733 (1998).

[53] G. S. Uhrig, New J. Phys. **10**, 083024 (2008).

[54] L. Cywinski, R. M. Lutchyn, C. P. Nave, and S. DasSarma, Phys. Rev. B **77**, 174509 (2008).

[55] G. S. Uhrig and D. A. Lidar, Phys. Rev. A **82**, 012301 (2010).

[56] A. Ajoy, G. A. Álvarez, and D. Suter (to be published.)

[57] G. S. Uhrig and S. Pasini, New J. Phys. **12**, 045001 (2010).

[58] S. Pasini, P. Karbach, C. Raas, and G. S. Uhrig, Phys. Rev. A **80**, 022328 (2009).